PCCP

ROYAL SOCIETY OF CHEMISTRY

PAPER

View Article Online
View Journal | View Issue

Cite this: *Phys. Chem. Chem. Phys.*, 2024, **26**, 9524

Pressure and temperature dependent kinetics and the reaction mechanism of Criegee intermediates with vinyl alcohol: a theoretical study†

Cuihong Sun, [a] Baoen Xu [a] and Yanli Zeng *[b]

Criegee intermediates (CIs), the key intermediates in the ozonolysis of olefins in atmosphere, have received much attention due to their high activity. The reaction mechanism of the most simple Criegee intermediate CH_2OO with vinyl alcohol (VA) was investigated by using the HL//M06-2X/def2TZVP method. The temperature and pressure dependent rate constant and product branching ratio were calculated using the master equation method. For CH_2OO + *syn*-VA, 1,4-insertion is the main reaction channel while for the CH_2OO + *anti*-VA, cycloaddition and 1,2-insertion into the O–H bond are more favorable than the 1,4-insertion reaction. The 1,4-insertion or cycloaddition intermediates are stabilized collisionally at 300 K and 760 torr, and the dissociation products involving OH are formed at higher temperature and lower pressure. The rate constants of the CH_2OO reaction with *syn*-VA and *anti*-VA both show negative temperature effects, and they are 2.95×10^{-11} and 2.07×10^{-13} cm^3 $molecule^{-1}$ s^{-1} at 300 K, respectively, and the former is agreement with the prediction in the literature.

Received 17th December 2023,
Accepted 26th February 2024

DOI: 10.1039/d3cp06115a

rsc.li/pccp

1. Introduction

Criegee intermediates (CIs) are also known as carbonyl oxides, the atmospheric intermediates produced in the oxidation of unsaturated hydrocarbons with ozone. In the ozonolysis reactions, the CI is formed vibrationally excited, and the energized CI will undergo rapid unimolecular decomposition or be stabilized collisionally and eventually be lost through bimolecular reactions or UV photolysis.[1,2]

Criegee intermediates may affect the oxidative capacity of the atmosphere by producing OH[3–7] and influencing the tropospheric HO_x budget, and they also play an important role in the formation of atmospheric aerosols[8,9] by reaction with SO_2,[10,11] which is an important gas-phase source of low-volatility sulfuric acid. As a 1,3-bipole radical with zwitterionic character, a Criegee intermediate can react with H_2O,[12–14] $(H_2O)_2$[14,15] NH_3,[16,17] alkane,[18–20] atmospheric organic and inorganic acids acids[21–26] and alcohols[27–31] *via* an insertion reaction, or react with SO_2,[32,33] carbonyl compounds,[34–37] and alkenes[38] *via* a cycloaddition reaction, or be associated with other 1,3-bipoles, such as ozone or carbonyl oxides.[39–42]

The major loss paths for Criegee intermediates are assumed to be the reactions with water vapor, which is ubiquitous throughout the troposphere while the CI reaction with H_2O is slow, and the rate constant is about 10^{-15}–10^{-16} cm^3 $molecule^{-1}$ s^{-1}.[43,44] The reaction of CIs + alcohols has a similar 1,2-insertion mechanism to that of CIs + H_2O, and the measured rate constants[31] by experiment for the simplest Criegee intermediate (CH_2OO) with methanol, ethanol, and 2-propanol are $(1.4 \pm 0.4) \times 10^{-13}$, $(2.3 \pm 0.6) \times 10^{-13}$, and $(1.9 \pm 0.5) \times 10^{-13}$ cm^3 $molecule^{-1}$ s^{-1}. Vereecken[22] investigated the reaction of CH_2OO with HNO_3 and HCOOH, and found that a 1,4-insertion mechanism allows for barrierless reactions with high rate constants up to $\sim 10^{-10}$ cm^3 $molecule^{-1}$ s^{-1}. He determined that the 1,4-insertion mechanism relies on the presence of a double bond in the α-position to the acidic OH group. The reactions of CI with enols were predicated to likewise react through the 1,4-insertion mechanism, with the rate constant exceeding 10^{-11} cm^3 $molecule^{-1}$ s^{-1}. Thus, the CH_2OO reaction with enols by 1,4-insertion will be much faster than with H_2O, methanol, ethanol, *etc.* using the 1,2-insertion mechanism.

Vinyl alcohol (VA) is the simplest enol, with high reactivity in atmospheric and combustion chemistry;[45] it has been implicated as a precursor to atmospheric carboxylic acids.[46–49] The main atmospheric decay channel of vinyl alcohol is the reaction

[a] *Shijiazhuang Key Laboratory of Low Carbon Energy Materials, Technology Innovation Center of HeBei for Heterocyclic Compound, College of Chemical Engineering, Shijiazhuang University, Shijiazhuang 050035, P. R. China*
[b] *College of Chemistry and Materials Science, Hebei Normal University, Shijiazhuang 050024, P.R. China. E-mail: yanlizeng@hebtu.edu.cn*

† Electronic supplementary information (ESI) available. See DOI: https://doi.org/10.1039/d3cp06115a

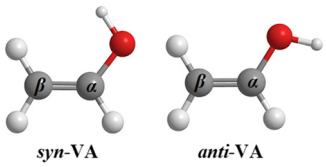

Scheme 1 Conformers of *syn*-VA and *anti*-VA.

with the OH radical, which has been incorporated into the atmospheric chemistry box model estimating the contribution of photo-tautomerization of acetaldehyde to the worldwide formic acid production.[49] Since organic acids are key species in the formation of secondary organic aerosol, the investigation on the bimolecular reaction of vinyl alcohol is of potential importance. Furthermore, the rate constant of VA + CH_2OO may be comparable or even faster than that of VA + OH (1.48×10^{-11}).[50] Under natural conditions, vinyl alcohol has two conformers, *syn*-VA and *anti*-VA, and the calculated *syn*/*anti* ratio is 85 : 15 at 300 K.[45] As shown in Scheme 1, both *syn*-VA and *anti*-VA display Cs symmetry. Theoretical study shows that the favorable OH-addition site for *syn*-VA is β-C, while for the *anti*-VA, the favorable OH-addition site is α-C.[50] Likewise, are the main reaction channels for CH_2OO with *syn*-VA and *anti*-VA both 1,4-insertion, or are there different mechanisms?

In this work, we studied the detailed reaction mechanism of CH_2OO with vinyl alcohol (*syn* and *anti*), including 1,4-insertion over the C=C–OH moiety, 1,2-insertion into the C–H or O–H bond, and cycloaddition across the C=C double bond. The rate constants and products' branching ratios were calculated using

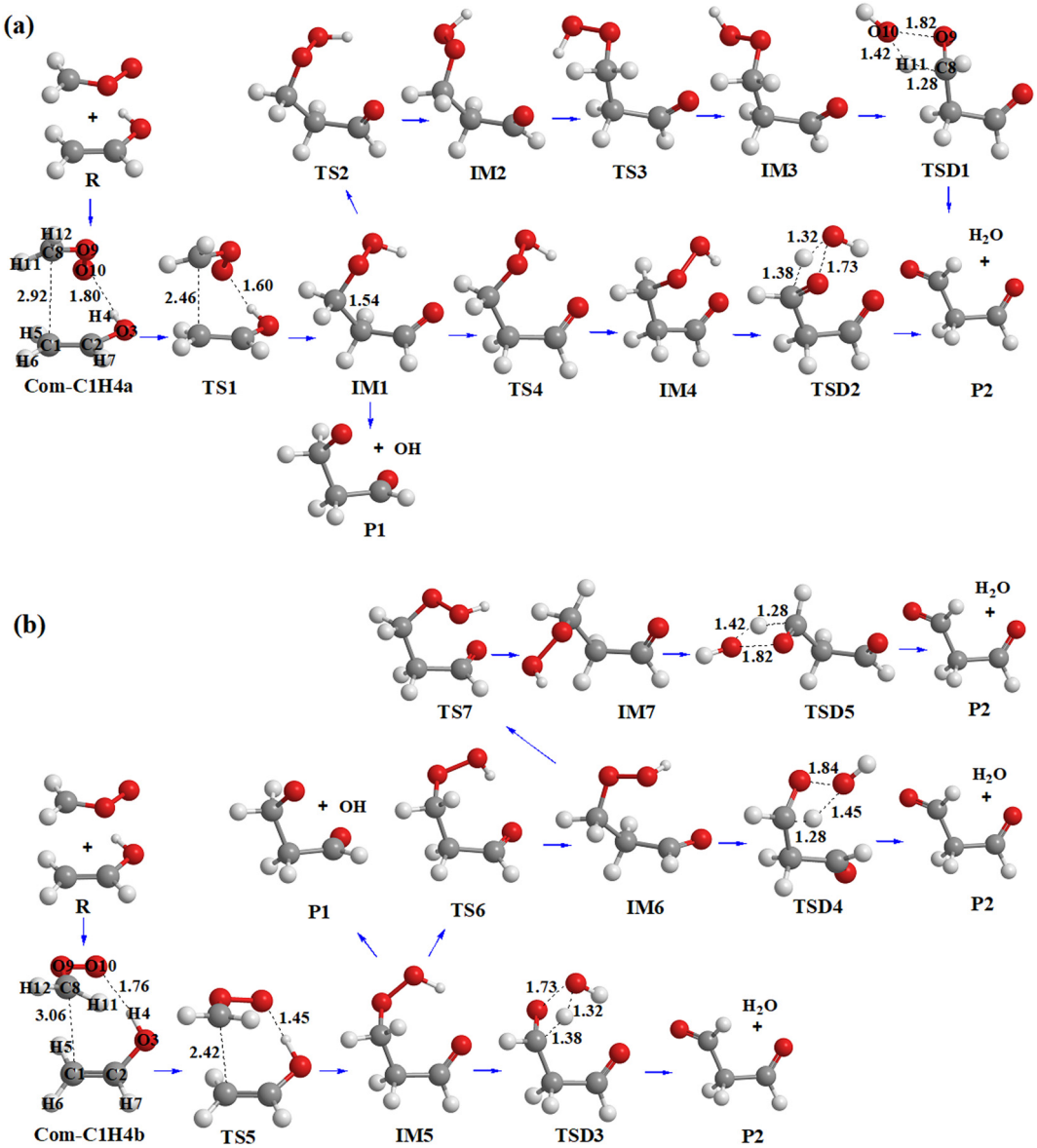

Fig. 1 The optimized geometries of stationary points in 1,4-insertion reactions for the CH_2OO + *syn*-VA reaction. (a) Channel initiates from Com-C1H4a; (b) Channel initiates from Com-C1H4b.

the master equation (ME) method, to determine the product distributions at different temperatures and pressures.

2. Computational method

2.1 Electronic structure calculations

The geometries of the reactants, pre-reactive complexes, transition states, and products of the title reaction were optimized at the M06-2X/def2TZVP level of theory. The harmonic vibration frequency was calculated at the same level of theory to obtain the zero-point energy (ZPE) and to verify the nature (minima or saddle points) of the stationary points. All transition states discussed in this work were verified by intrinsic reaction coordinate (IRC) calculations to identify the reactants and products. The single-point energies of all stationary points were then refined by a higher-level (denoted as HL) single-point energy calculation method. The HL energies were obtained *via* a combination of coupled cluster calculations with perturbative inclusion of the triplet contribution, CCSD(T),[51] and second order Moller–Plesset perturbation theory (MP2).[52,53] The complete basis set limit energy was estimated by the extrapolation of results obtained for sequences of the correlation-consistent polarized-valence basis sets. The expression for this method can be as follows:

$$E_{HL} = E[\text{CCSD(T)/cc-pVTZ}] + (E[\text{CCSD(T)/cc-pVTZ}] - E[\text{CCSD(T)/cc-pVDZ}]) \times 0.46286 + E[\text{MP2(FC)/cc-pVQZ}] + (E[\text{MP2(FC)/cc-pVQZ}] - E[\text{MP2(FC)/cc-pVTZ}]) \times 0.69377 - E[\text{MP2(FC)/cc-pVTZ}] - (E[\text{MP2(FC)/cc-pVTZ}] - E[\text{MP2(FC)/cc-pVDZ}]) \times 0.46286$$

The HL method has been verified to be accurate for both closed shell and open shell species' calculations.[54,55] The rate constants of Criegee intermediates with acrolein and C_2H_4 reactions[35,56] based on the HL potential energy surface have been proved to be consistent with experimental results. All the electronic structure and energetic calculations were carried out using the Gaussian 09 program package.[57]

2.2 Kinetic calculations

The rate constant and products' branching ratios were calculated using the master equation method,[58–62] which is a powerful tool for calculating the temperature and pressure dependent

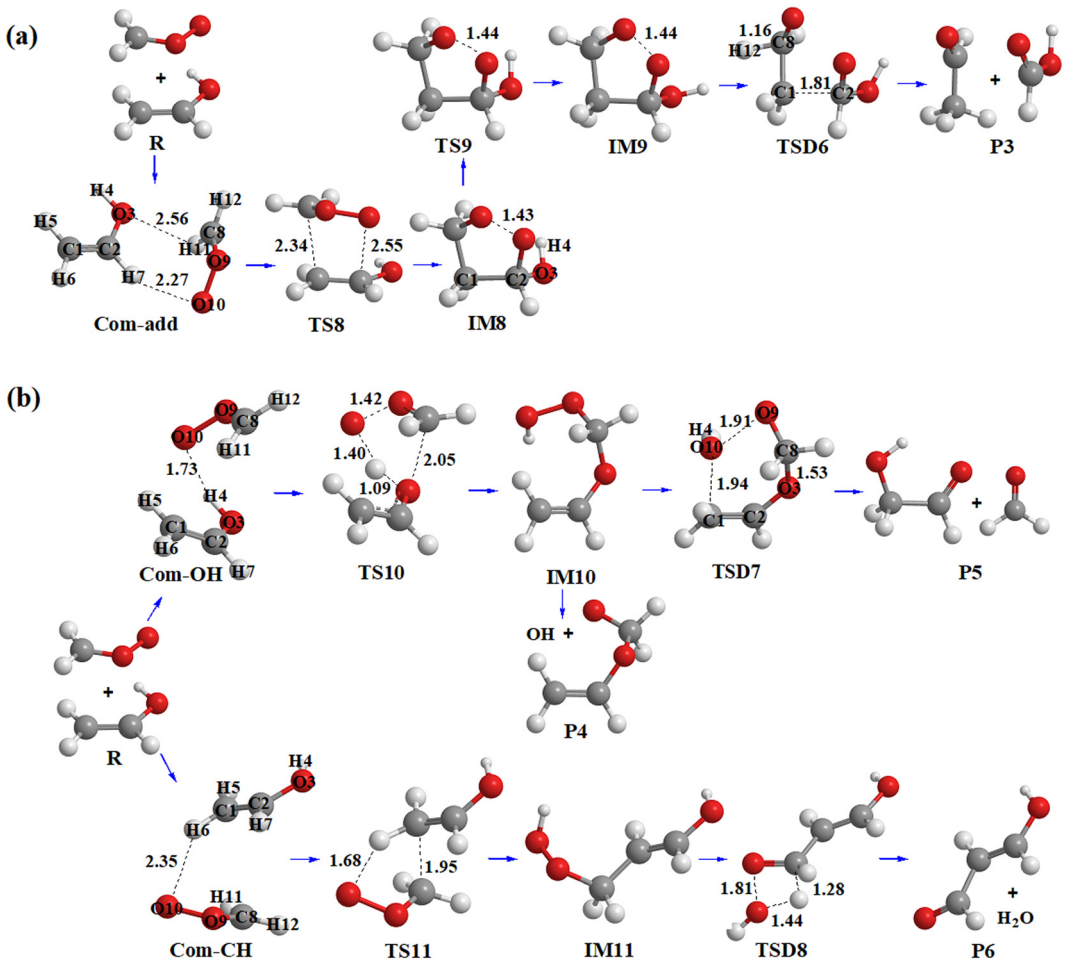

Fig. 2 The optimized geometries of stationary points for the CH_2OO + *syn*-VA reaction. (a) Cycloaddition reaction; (b) 1,2-insertion reaction in O–H and C–H bonds.

kinetics of a multiple-channel and multiple-well chemical reaction system. Energy transfer is treated with the single exponential down model with ΔE_{down} = 200 cm^{-1}. The Lennard-Jones (L-J) parameters of the intermediates $C_3O_3H_6$ (σ = 6.0 Å and ε/k_b = 450 K) are taken from ref. 63 and the L-J parameters of N_2 are taken as σ = 3.9 Å and ε/k_b = 48 K.[58] In order to evaluate the sensitivity of the results for the L-J parameters of the intermediates, σ = 4.5 Å and ε/k_b = 350 K[22] are used to recalculated the rate constant for comparison, and the results show no obvious change. In this study, the master equation was solved by an ordinary differential equation (ODE) solver to develop directly the number population of the species with time.[64–66] The populations of species as functions of time can be obtained directly and the first-order rate constants can be extracted from the reactant population using the ''exponential decay'' approach. More details and test cases can be found in ref. 55 and 66–68. All the kinetic calculations were carried out by using TheRate program.[69]

3. Results and discussion

3.1. Reaction mechanism of CH_2OO + *syn*-VA

The optimized geometries of pre-reactive complexes, transition states, intermediates, and products are shown in Fig. 1 and 2. The PES for the CH_2OO + *syn*-VA reaction is portrayed in Fig. 3. All the reaction channels initiate from the pre-reactive complex, and they are named Com-C1H4a (Com-C1H4b) for the

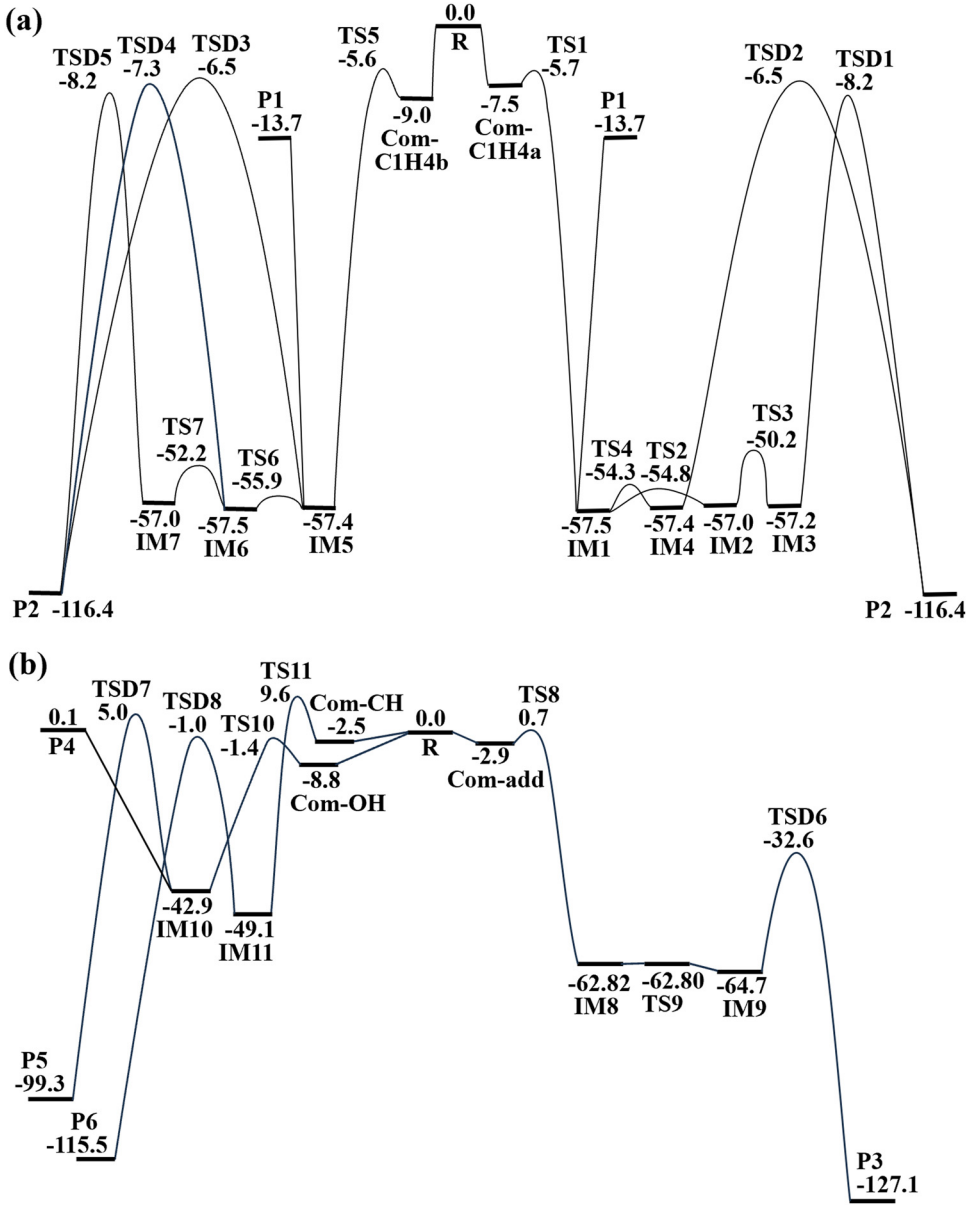

Fig. 3 PES of CH_2OO + *syn*-VA reaction at the HL//M06-2X/def2TZVP level of theory. The relative energies are given in kcal mol^{-1}. (a) 1,4-insertion reaction; (b) cycloaddition and 1,2-insertion reactions in O–H and C–H bonds.

1,4-insertion reaction, Com-add for the cycloaddition reaction, Com-OH and Com-CH for the O–H and C–H 1,2-insertion reaction, respectively.

For the 1,4-insertion reaction over the C═C–OH moiety, the CH_2OO carbon atom and the terminal oxygen atom approaches the β-C and the hydroxyl H atom of *syn*-VA respectively, forming the pre-reactive complexes Com-C1H4a and Com-C1H4b, which are 7.5 and 9.0 kcal mol^{-1} more stable than the free reactants. In Com-C1H4a, the central oxygen atom (O9) of CH_2OO lies on the same side with hydroxyl O atom (O3) of *syn*-VA, while in Com-C1H4b, they lie on the opposite side.

As shown in Fig. 1(a) and 3(a), starting from Com-C1H4a, the CH_2OO carbon atom attacks *β*-C and the hydroxyl H atom shifts to the terminal oxygen of CH_2OO forming the intermediate IM1 (3-hydroperoxy-propanal), the relative energies of TS1 and IM1 are −5.7 and −57.5 kcal mol^{-1}. The energized 3-hydroperoxy-propanal can dissociate directly to $CHOCH_2CH_2O$ + OH (P1, −13.7 kcal mol^{-1}), or it will proceed *via* two different isomerization and decomposition pathways to form the same product P2 (H_2O + malondialdehyde). Firstly, IM1 isomerizes to IM3 by the rotation of –CHO (TS2, −54.8 kcal mol^{-1}) and –OH groups (TS3, −50.2 kcal mol^{-1}), and then decomposes to P2 by the dissociation of the O9–O10 bond accompanied by H11 shifting from C8 to O10 (TSD1, −8.2 kcal mol^{-1}). Secondly, IM1 isomerizes to IM4 by the molecular skeleton rotation (TS4, −54.3 kcal mol^{-1}) to facilitate the subsequent H1 atom shift from C8 to O10, and then decomposes to P2 by H shift and O–O bond fission (TSD2, −6.5 kcal mol^{-1}). The relative energies of the local minima IM2, IM3, IM4, and P2 are −57.0, −57.2, −57.4, and −116.4 kcal mol^{-1}, respectively. The dissociation to $CHOCH_2CH_2O$ + OH may be energetically more favorable due to the high-energy TSD1 and TSD2 in the formation of H_2O + malondialdehyde.

As shown in Fig. 1(b) and 3(a), starting from Com-C1H4b, the 1,4-insertion of CH_2OO over C═C–OH moiety forms the intermediate IM5 *via* TS5, the respective relative energy of TS5 and IM5 are −5.6 and −57.4 kcal mol^{-1}. IM5 can isomerize to IM6 (−57.5 kcal mol^{-1}) by rotation of –CHO and –OH (TS6, −55.9 kcal mol^{-1}), and IM6 then isomerizes to IM7 (−57.0 kcal mol^{-1}) by molecular skeleton rotation (TS7, −52.2 kcal mol^{-1}). IM5, IM6, and IM7 can all decompose to H_2O and malondialdehyde, and the relative energies of the corresponding transition state TSD3, TSD4, and TSD5 are −6.5, −7.3 and −8.2 kcal mol^{-1}, respectively. Likewise, IM5 can also form $CHOCH_2CH_2O$ + OH by direct dissociation.

For the cycloaddition reaction on the C═C double bond, the formation of a five-membered adduct IM8 (−62.8 kcal mol^{-1}) needs to overcome an energy barrier of 0.7 kcal mol^{-1}. As shown in Fig. 2(a), IM8 isomerizes to IM9 (−64.7 kcal mol^{-1}) by the –OH group rotation around C–O bond (TS9), and then IM9 decomposes to products aldehyde and formic acid (P3, −127.1 kcal mol^{-1}) by C1–C2 bond breakage and H12 migration from C8 to C1. It is worth mentioning that the electronic

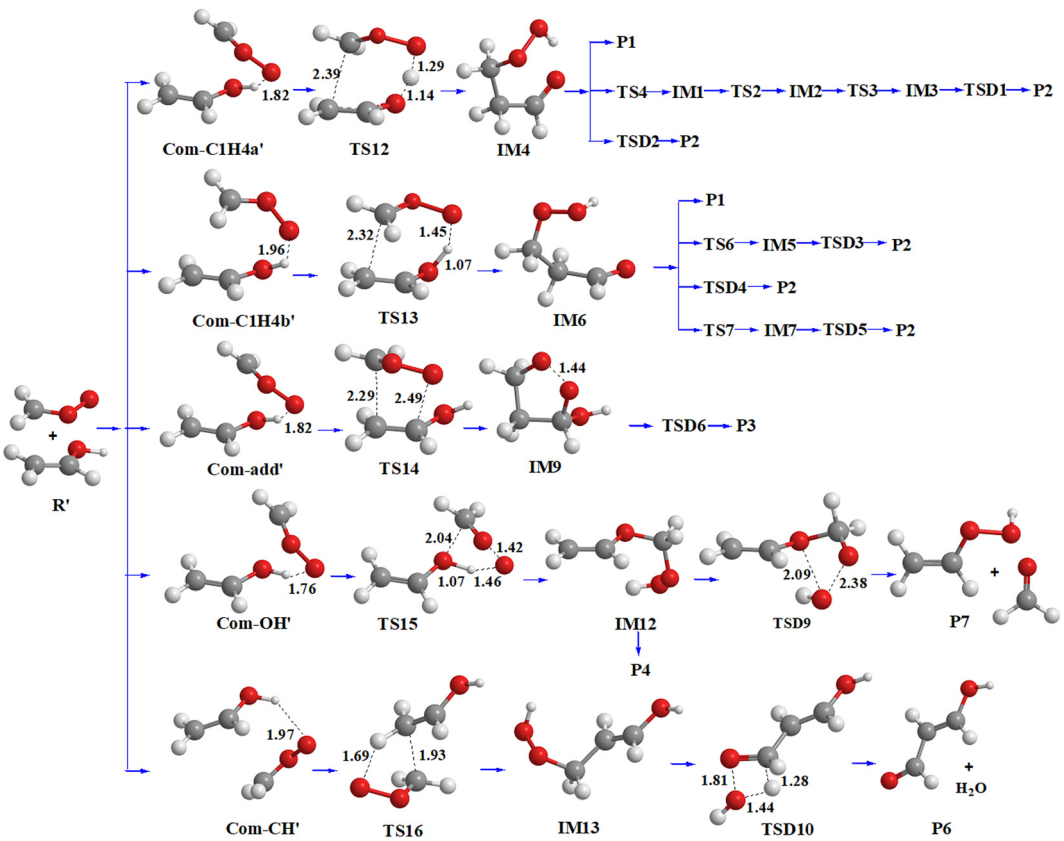

Fig. 4 The optimized geometries of stationary points for the CH_2OO + *anti*-VA reaction.

energy of TS9 is only 0.02 kcal mol^{-1} higher than that of IM8, and the PES from IM8 to TS9 is very flat, which leads to the sum of electronic and zero-point energies of TS9 being slightly lower than IM8. Therefore, only the electronic portion is used to compute the relative height of TS9 to IM8 in this work. For clarity, the relative energy values of IM8 and TS9 in Fig. 3 are kept to two decimal places. The vector of the imaginary frequency in TS9 is the OH rotation around the C–O bond (Fig. S1, ESI†), and the dihedral angle C1C2O3H4 is 73.0, 80.8, and 164.2° in IM8, TS9, and IM9, respectively. The Cartesian coordinates of IM8 and TS9 are shown in the ESI† (Table S1).

The 1,2-insertion in the O–H bond is a barrierless pathway leading to IM10 with 42.9 kcal mol^{-1} exoergicity, IM10 may decompose directly to CH_2CHOCH_2O + OH (P4, 0.1 kcal mol^{-1}), or form CH_2OHCHO + HCHO (P5, −99.3 kcal mol^{-1}) *via* the O3–C8 bond breakage and O10H4 shift from O9 to C1. The 1,2-insertion in the C–H bond needs to overcome the 9.6 kcal mol^{-1} energy barrier, so it has a negligible contribution compared to other channels.

Comparing the PESs of all the channels in the CH_2OO + *syn*-VA reactions (Fig. 3), we found that all the stationary points in the 1,4-insertion reaction lie below the reactants, and the entrance is barrierless for the 1,4-insertion reaction and 1,2-insertion in the O–H bond. So the 1,4-insertion reaction is more competitive than other channels.

3.2. Reaction mechanism of CH_2OO + *anti*-VA

The optimized geometries of the stationary points in CH_2OO + *anti*-VA reaction are shown in Fig. 4, and the PES are shown in Fig. 5. Similar to the CH_2OO + *syn*-VA reaction, all the reaction channels initiate from the pre-reactive complex, and the

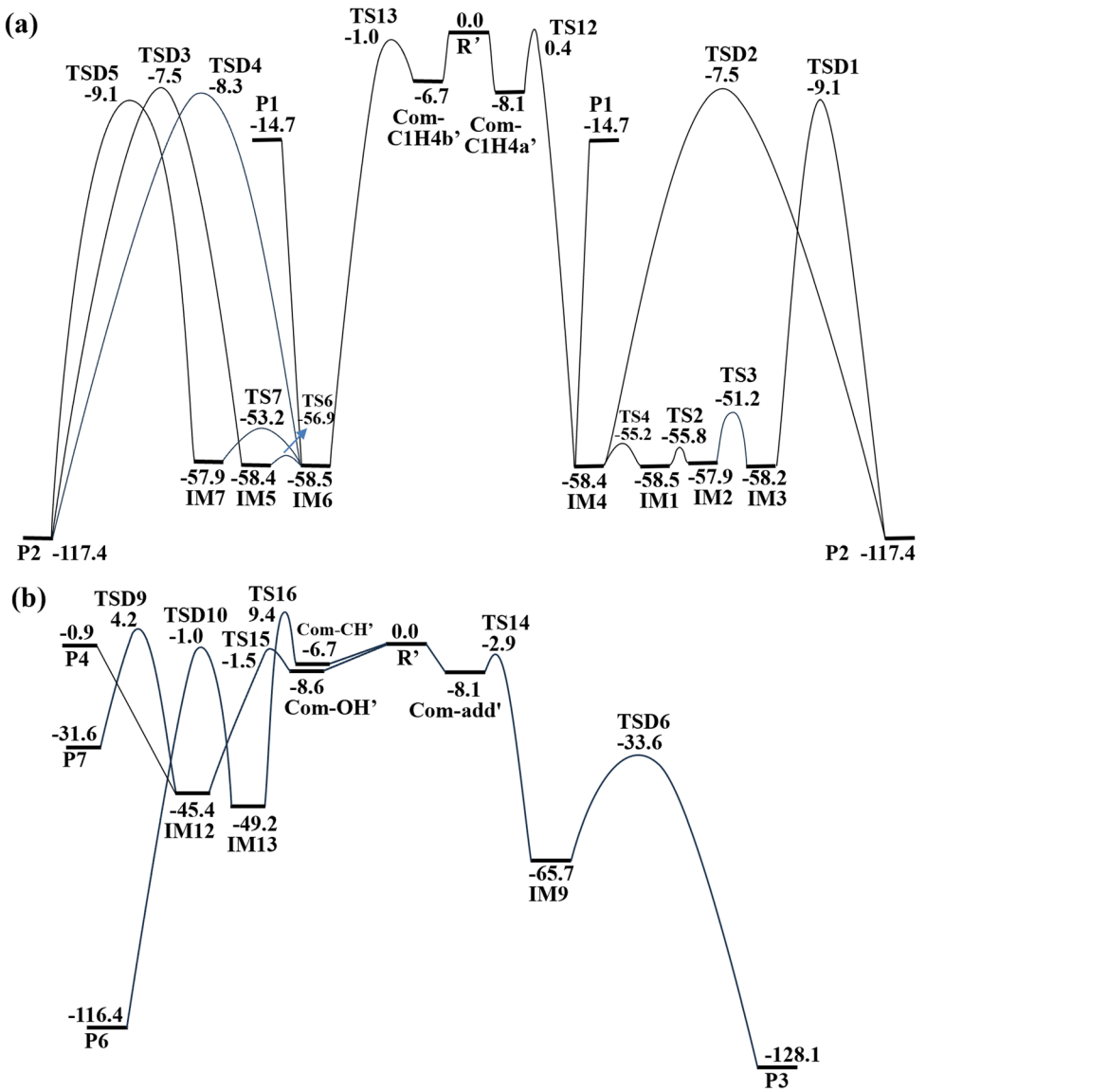

Fig. 5 PES of the CH_2OO + *anti*-VA reaction at the HL//M06-2X/def2TZVP level of theory. The relative energies are given in kcal mol^{-1}. (a) 1,4-insertion reactions; (b) cycloaddition and 1,2-insertion reaction in O–H and C–H bonds.

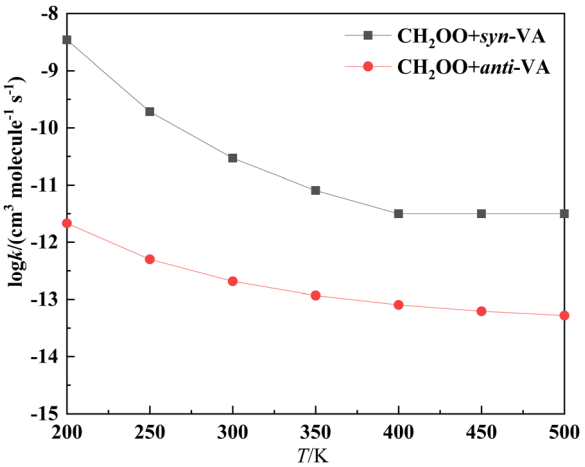

Fig. 6 The rate constants of the CH_2OO + *syn*-VA and CH_2OO + *anti*-VA reactions at 200–500 K and 760 torr.

corresponding complexes are named Com-C1H4a′ (Com-C1H4b′), Com-add′, Com-OH′ and Com-CH′, respectively.

Starting from Com-C1H4a′ and Com-C1H4b′, the 1,4-insertion of CH_2OO into *anti*-VA forms the intermediates IM4 and IM6, respectively. Both IM4 and IM6 can dissociate directly to $CHOCH_2CH_2O$ + OH. IM4 can isomerize to IM1, IM2, and IM3 successively, IM6 can isomerize to IM5 or IM7, and then IM3, IM4, IM5, IM6, and IM7 decomposes to the product P2 (H_2O + malondialdehyde). The cycloaddition reaction of CH_2OO + *anti*-VA forms the adducts IM9 firstly, and IM9 can decompose to the product P3 *via* TSD6. The optimized structures of IM1–IM9, and their isomerization and dissociation processes have been described in detail in the CH_2OO + *syn*-VA reaction. The O–H and C–H 1,2-insertion reaction results in the formation of respective intermediates IM12 and IM13 and decomposition to the corresponding products P4 (or P7) and P6.

From Fig. 5 we can see that the energies of the stationary points in the cycloaddition and 1,4-insertion reaction are obviously lower than those in other channels. In addition, TS14 (−2.9 kcal mol^{-1}) in the entrance channel of cycloaddition has lower energy than TS12 and TS13 (0.4 and −1.0 kcal mol^{-1}) in the 1,4-insertion reaction. So, the cycloaddition may be favorable in the CH_2OO + *anti*-VA reaction, which is different from the CH_2OO + *syn*-VA reaction.

3.3. Kinetic calculations

The master equation calculations were carried out at the pressure range of 1–760 torr and the temperature range of 200–500 K. According to the reaction PESs, the 1,4-insertion reaction, cycloaddition reaction, and 1,2-insertion reaction in O–H are involved in the master equation calculation, while the 1,2-insertion reaction in C–H bond are excluded because of its higher reaction energy barrier. The calculated TS from the pre-reactive complex is approximately taken as the bottleneck for the present reaction system. The reactants are assumed to be in fast equilibrium with the pre-reactive complex (C), and the rate constant of C → P is much smaller than that of C → CH_2OO + vinyl alcohol, like the treatment in a barrierless entrance reaction system.[70–72]

3.3.1 Rate constants. The calculation results show that the rate constants are pressure independent. Fig. 6 portrays the rate constants of CH_2OO + *syn*-VA and CH_2OO + *anti*-VA at 200–500 K and 760 torr, and the values are listed in Table 1. We can see that the rate constants decline with the increase of the temperature, *i.e.*, they show negative temperature effects, and this results from their barrierless entrance step. At 300 K and 760 torr, the rate constants of CH_2OO + *syn*-VA and CH_2OO + *anti*-VA are 2.95×10^{-11} and 2.07×10^{-13} cm^3 $molecule^{-1}$ s^{-1}, respectively. Vereecken has predicted that the rate constant of CI + VA should easily exceed 1×10^{-11} cm^3 $molecule^{-1}$ s^{-1}, which is agreement with our calculation results of CH_2OO + *syn*-VA. The traditional transition state theory (TST) is used to calculate the rate constants of each entrance channel, and the overall rate constants (Table S2, ESI†) are consistent with those calculated by the master equation method.

3.3.2 Products' branching ratios. For the 1,4-insertion intermediate, the direct dissociation to $CHOCH_2CH_2O$ + OH may be more competitive than the formation of malondialdehyde + H_2O.[22,73] However, this ratio is hard to estimate due to the direct dissociation to $CHOCH_2CH_2O$ + OH without a well-defined transition state. So we located the approximate minimum energy path (MEP) and determined the minima of the TST rate constants along the MEP. The corresponding structure of the minima of TST rate constants was taken as the variational transition state and used to the subsequent master equation calculation to evaluate the product distribution. This is similar to the variational approach applied to the barrierless reactions by Lin *et al.*[74,75] The location of minimum energy path and the variation of TST rate constants for the dissociation process are given in Fig. S2 (ESI†).

For the CH_2OO + *syn*-VA reaction, the calculation results show that the both the 1,2-insertion and the cycloaddition reaction are negligible compared to the 1,4-insertion reaction. As shown in Fig. 7 and 8, the domain product is the 1,4-insertion intermediate (3-hydroperoxy-propanal) thermalized in collisions with the bath gas at 300 K and 760 torr. The pressure dependence of the products' branching ratios is obvious at lower pressure ranges. The intermediates IM1–IM7

Table 1 Values of the rate constants *k* (in cm^3 $molecule^{-1}$ s^{-1}) for the CH_2OO + VA reaction at 200–500 K and 760 torr

Temperature	200	250	300	350	400	450	500
k (CH_2OO + *syn*-VA)	3.44×10^{-9}	1.92×10^{-10}	2.95×10^{-11}	8.05×10^{-12}	3.14×10^{-12}	3.14×10^{-12}	3.14×10^{-12}
k (CH_2OO + *anti*-VA)	2.15×10^{-12}	5.01×10^{-13}	2.07×10^{-13}	1.17×10^{-13}	8.04×10^{-14}	6.22×10^{-14}	5.23×10^{-14}

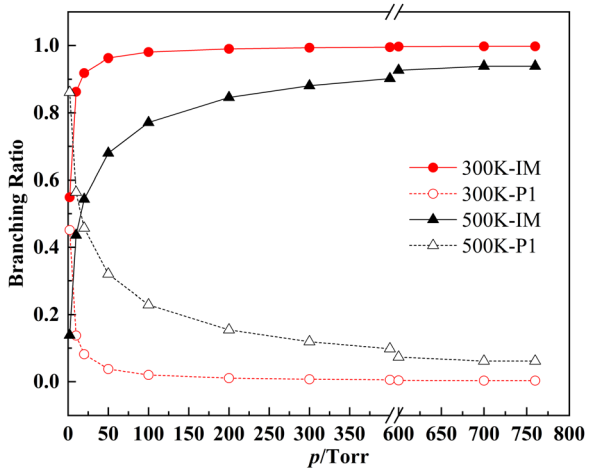

Fig. 7 The branching ratios of the products for the CH_2OO + *syn*-VA reaction.

are shown in Fig. 7 as a whole for clarity, and the individual branching ratios for IM1–IM7 at 300 K and 1 torr, 100 torr and 760 torr are shown in Fig. 8. The ratios of IM1–IM7 are in the order IM6 > IM1 > IM4 > IM5 > IM3 > IM2 > IM7, which are determined by their relative energies (−57.5, −57.5, −57.4, −57.4, −57.2, −57.0, and −57.0 kcal mol^{-1}). The 1,4-insertion intermediate decomposes to $CHOCH_2CH_2O$ + OH at higher temperature and lower pressure, and the products malondialdehyde + H_2O are negligible.

The products' branching ratios of the CH_2OO + *anti*-VA reaction are shown in Fig. 9. The dominant product is the cycloaddition intermediate IM9, and it dissociates to P3 (aldehyde and formic acid) gradually with the increase of temperature and the decrease of pressure, and, in the meanwhile, the direct dissociation product P4 (CH_2CHOCH_2O + OH) of the O–H 1,2-insertion intermediate IM12 has a significant contribution.

Combining the PESs and the kinetic characters of the two reactions, we find that the 1,4-insertion dominated the CH_2OO + *syn*-VA reaction, while the cycloaddition and O–H 1,2-insertion are more favorable in the CH_2OO + *anti*-VA reaction. At 300 K and 760 torr, the 1,4-insertion or cycloaddition intermediates are the main products. At higher temperature and lower pressure, the 1,4-insertion intermediate tends to decompose to $CHOCH_2CH_2O$ + OH, so the reaction can be regarded as the OH reservoir, and affect the HO_x budget, thereby having a potential impact on the oxidative capacity of the atmosphere. In addition, the reaction of CH_2OO with vinyl alcohol is significantly faster than CH_2OO + saturated alcohol ($\sim 10^{-13}$ cm^3 $molecule^{-1}$ s^{-1}),[31] and is comparable to the OH + vinyl alcohol reaction (1.48×10^{-11}),[50] due to the zwitterionic character of CH_2OO and special structure of vinyl alcohol, with a double bond in the α-position of the OH group. So this reaction may be an important loss process for both Criegee intermediate and vinyl alcohol.

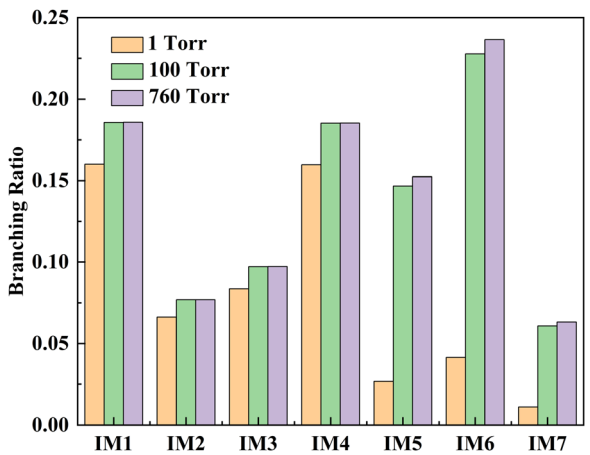

Fig. 8 The branching ratios of the IM1–IM7 in the CH_2OO + *syn*-VA reaction at 300 K and 1 torr, 100 torr and 760 torr.

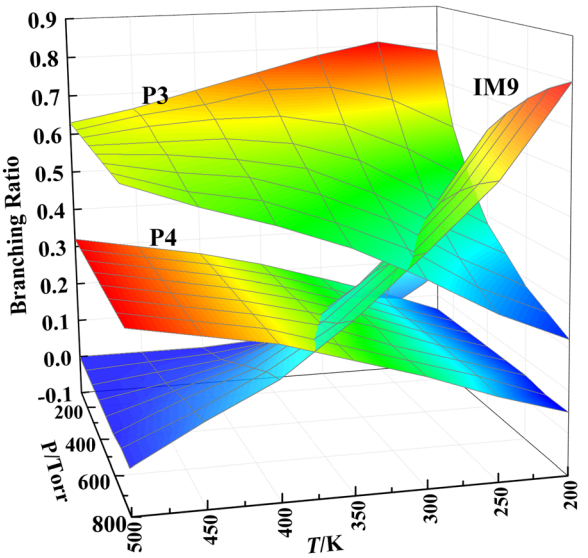

Fig. 9 The branching ratios of the products for the CH_2OO + *anti*-VA reaction.

4. Conclusions

The reaction mechanism of CH_2OO with vinyl alcohol has been investigated at the HL//M06-2X/def2TZVP level of theory. The calculation results of the master equation method reveal the temperature and pressure dependent kinetic characters. The following conclusions can be drawn. (1) The 1,4-insertion reaction is the main channel for the CH_2OO + *syn*-VA reaction, while the cycloaddition is more competitive in the CH_2OO + *anti*-VA reaction. (2) The rate constants are 2.95×10^{-11} and 2.07×10^{-13} cm^3 $molecule^{-1}$ s^{-1} for CH_2OO + *syn*-VA and CH_2OO + *anti*-VA reactions at 300 K and 760 torr, and both show negative temperature effects at 200–500 K. (3) The product distribution is temperature and pressure dependent. At 300 K and 760 torr, the 3-hydroperoxy-propanal formed by 1,4-insertion in the CH_2OO + *syn*-VA reaction and the cycloaddition intermediate in the CH_2OO + *anti*-VA reaction are main

products. At higher temperature and lower pressure, 3-hydroperoxy-propanal dissociates to $CHOCH_2CH_2O$ + OH, and cycloaddition intermediate decomposes to aldehyde and formic acid; in the meanwhile, CH_2CHOCH_2O + OH are formed by the dissociation of 1,2-insertion (in O-H bond) intermediate in CH_2OO + *anti*-VA reaction.

Conflicts of interest

There are no conflicts to declare.

Acknowledgements

This work was funded by the National Natural Science Foundation of China (No. 21603152), the Natural Science Foundation of Hebei Province (B2022205022), and the Science Research Project of Hebei Education Department (ZD2022157). We would also like to thank professor S. W. Zhang for providing technical support on the kinetic calculation of the CH_2OO + vinyl alcohol reaction.

References

1 P. Neeb, O. Horie and G. K. Moortgat, *J. Phys. Chem. A*, 1998, **102**, 6778–6785.
2 D. Johnson and G. Marston, *Chem. Soc. Rev.*, 2008, **37**, 699–716.
3 K. Samanta, J. M. Beames, M. I. Lester and J. E. Subotnik, *J. Chem. Phys.*, 2014, **141**, 134303.
4 F. Liu, J. M. Beames, A. S. Petit, A. B. McCoy and M. I. Lester, *Science*, 2014, **345**, 1596–1598.
5 A. Novelli, L. Vereecken, J. Lelieveld and H. Harder, *Phys. Chem. Chem. Phys.*, 2014, **16**, 19941–19951.
6 M. I. Lester and S. J. Klippenstein, *Acc. Chem. Res.*, 2018, **51**, 978–985.
7 V. P. Barber, S. Pandit, A. M. Green, N. Trongsiriwat, P. J. Walsh, S. J. Klippenstein and M. I. Lester, *J. Am. Chem. Soc.*, 2018, **140**, 10866–10880.
8 Y. Gong and Z. Chen, *Atmos. Chem. Phys.*, 2021, **21**, 813–829.
9 F. Bianchi, J. Tröstl, H. Junninen, C. Frege, S. Henne, C. R. Hoyle, U. Molteni, E. Herrmann, A. Adamov, N. Bukowiecki, X. Chen, J. Duplissy, M. Gysel, M. Hutterli, J. Kangasluoma, J. Kontkanen, A. Kürten, H. E. Manninen, S. Münch, O. Peräkylä, T. Petäjä, L. Rondo, C. Williamson, E. Weingartner, J. Curtius, D. R. Worsnop, M. Kulmala, J. Dommen and U. Baltensperger, *Science*, 2016, **352**, 1109–1112.
10 H.-L. Huang, W. Chao and J. J.-M. Lin, *Proc. Natl. Acad. Sci.*, 2015, **112**, 10857–10862.
11 L. Vereecken, *Science*, 2013, **340**, 154–155.
12 Y.-J. Wu, K. Takahashi and J. J.-M. Lin, *J. Phys. Chem. A*, 2023, **127**, 8059–8072.
13 B. Long, J. L. Bao and D. G. Truhlar, *J. Am. Chem. Soc.*, 2016, **138**, 14409–14422.
14 L.-C. Lin, H.-T. Chang, C.-H. Chang, W. Chao, M. C. Smith, C.-H. Chang, J. J.-M. Lin and K. Takahashi, *Phys. Chem. Chem. Phys.*, 2016, **18**, 4557–4568.
15 W. Chao, J.-T. Hsieh, C.-H. Chang and J. J.-M. Lin, *Science*, 2015, **347**, 751–754.
16 A. Nazari and V. Saheb, *Theor. Chem. Acc.*, 2022, **141**, 66.
17 B. Long, Y. Wang, Y. Xia, X. He, J. L. Bao and D. G. Truhlar, *J. Am. Chem. Soc.*, 2021, **143**, 8402–8413.
18 K. Xu, W. Wang, W. Wei, W. Feng, Q. Sun and P. Li, *J. Phys. Chem. A*, 2017, **121**, 7236–7245.
19 T. V. T. Mai, M. v Duong, H. T. Nguyen, K. C. Lin and L. K. Huynh, *Chem. Phys. Lett.*, 2018, **706**, 280–284.
20 L. Franzon, J. Peltola, R. Valiev, N. Vuorio, T. Kurtén and A. Eskola, *J. Phys. Chem. A*, 2023, **127**, 477–488.
21 O. Welz, A. J. Eskola, L. Sheps, B. Rotavera, J. D. Savee, A. M. Scheer, D. L. Osborn, D. Lowe, A. Murray Booth, P. Xiao, H. K. M. Anwar, C. J. Percival, D. E. Shallcross and C. A. Taatjes, *Angew. Chem., Int. Ed.*, 2014, **53**, 4547–4750.
22 L. Vereecken, *Phys. Chem. Chem. Phys.*, 2017, **19**, 28630–28640.
23 E. S. Foreman, K. M. Kapnas and C. Murray, *Angew. Chem., Int. Ed.*, 2016, **55**, 10419–10422.
24 R. Chhantyal-Pun, M. R. McGillen, J. M. Beames, M. A. H. Khan, C. J. Percival, D. E. Shallcross and A. J. Orr-Ewing, *Angew. Chem., Int. Ed.*, 2017, **56**, 9044–9047.
25 P. Raghunath, Y. P. Lee and M. C. Lin, *J. Phys. Chem. A*, 2017, **121**, 3871–3878.
26 C. A. Chung, J. W. Su and Y. P. Lee, *Phys. Chem. Chem. Phys.*, 2019, **21**, 21445–21455.
27 W. Chao, Y.-H. Lin, C. Yin, W.-H. Lin, K. Takahashi and J. J.-M. Lin, *Phys. Chem. Chem. Phys.*, 2019, **21**, 13633–13640.
28 S. Enami and A. J. Colussi, *J. Phys. Chem. A*, 2017, **121**, 5175–5182.
29 M. R. McGillen, B. F. E. Curchod, R. Chhantyal-Pun, J. M. Beames, N. Watson, M. A. H. Khan, L. McMahon, D. E. Shallcross and A. J. Orr-Ewing, *ACS Earth Space Chem.*, 2017, **1**, 664–672.
30 Y.-H. Lin, C. Yin, W.-H. Lin, Y.-L. Li, K. Takahashi and J. J.-M. Lin, *J. Phys. Chem. Lett.*, 2018, **9**, 7040–7044.
31 S. V. Tadayon, E. S. Foreman and C. Murray, *J. Phys. Chem. A*, 2018, **122**, 258–268.
32 L. Vereecken, H. Harder and A. Novelli, *Phys. Chem. Chem. Phys.*, 2012, **14**, 14682–14695.
33 N. U. M. Howes, Z. S. Mir, M. A. Blitz, S. Hardman, T. R. Lewis, D. Stone and P. W. Seakins, *Phys. Chem. Chem. Phys.*, 2018, **20**, 22218–22227.
34 A. J. Eskola, M. Dontgen, B. Rotavera, R. L. Caravan, O. Welz, J. D. Savee, D. L. Osborn, D. E. Shallcross, C. J. Percival and C. A. Taatjes, *Phys. Chem. Chem. Phys.*, 2018, **20**, 19373–19381.
35 C. Sun, S. Zhang, J. Yue and S. Zhang, *J. Phys. Chem. A*, 2018, **122**, 8729–8737.
36 P.-B. Wang, D. G. Truhlar, Y. Xia and B. Long, *Phys. Chem. Chem. Phys.*, 2022, **24**, 13066–13073.
37 Y. Wei, Q. Zhang, X. Huo, W. Wang and Q. Wang, *Chemosphere*, 2022, **296**, 133717.

38 Z. J. Buras, R. M. Elsamra, A. Jalan, J. E. Middaugh and W. H. Green, *J. Phys. Chem. A*, 2014, **118**, 1997–2006.
39 L. Vereecken, H. Harder and A. Novelli, *Phys. Chem. Chem. Phys.*, 2014, **16**, 4039–4049.
40 Z. J. Buras, R. M. Elsamra and W. H. Green, *J. Phys. Chem. Lett.*, 2014, **5**, 2224–2228.
41 L. Vereecken, A. R. Rickard, M. J. Newland and W. J. Bloss, *Phys. Chem. Chem. Phys.*, 2015, **17**, 23847–23858.
42 R. Chhantyal-Pun, A. Davey, D. E. Shallcross, C. J. Percival and A. J. Orr-Ewing, *Phys. Chem. Chem. Phys.*, 2015, **17**, 3617–3626.
43 D. Stone, M. Blitz, L. Daubney, N. U. Howes and P. Seakins, *Phys. Chem. Chem. Phys.*, 2014, **16**, 1139–1149.
44 T. Berndt, R. Kaethner, J. Voigtlander, F. Stratmann, M. Pfeifle, P. Reichle, M. Sipila, M. Kulmala and M. Olzmann, *Phys. Chem. Chem. Phys.*, 2015, **17**, 19862–19873.
45 M. F. Shaw, D. L. Osborn, M. J. T. Jordan and S. H. Kable, *J. Phys. Chem. A*, 2017, **121**, 3679–3688.
46 D. U. Andrews, B. R. Heazlewood, A. T. Maccarone, T. Conroy, R. J. Payne, M. J. Jordan and S. H. Kable, *Science*, 2012, **337**, 1203–1206.
47 A. T. Archibald, M. R. McGillen, C. A. Taatjes, C. J. Percival and D. E. Shallcross, *Geophys. Res. Lett.*, 2007, **34**, L21801.
48 S. So, U. Wille and G. da Silva, *Environ. Sci. Technol.*, 2014, **48**, 6694–6701.
49 M. F. Shaw, B. Sztaray, L. K. Whalley, D. E. Heard, D. B. Millet, M. J. T. Jordan, D. L. Osborn and S. H. Kable, *Nat. Commun.*, 2018, **9**, 2584.
50 X. Lei, W. Wang, J. Cai, C. Wang, F. Liu and W. Wang, *J. Phys. Chem. A*, 2019, **123**, 3205–3213.
51 G. E. Scuseria, C. L. Janssen and H. F. Schaefer, III, *J. Chem. Phys.*, 1988, **89**, 7382–7387.
52 C. Møller and M. S. Plesset, *Phys. Rev.*, 1934, **46**, 618–622.
53 M. Head-Gordon, J. A. Pople and M. J. Frisch, *Chem. Phys. Lett.*, 1988, **153**, 503–506.
54 J. A. Miller and S. J. Klippenstein, *J. Phys. Chem. A*, 2003, **107**, 2680–2692.
55 C. H. Sun, B. E. Xu and S. W. Zhang, *J. Phys. Chem. A*, 2014, **118**, 3541–3551.
56 C. Sun, B. Xu, L. Lv and S. Zhang, *Phys. Chem. Chem. Phys.*, 2019, **21**, 16583–16590.
57 M. J. Frisch, G. W. Trucks, H. B. Schlegel, G. E. Scuseria, M. A. Robb, J. R. Cheeseman, G. Scalmani, V. Barone, B. Mennucci, G. A. Petersson, H. Nakatsuji, M. Caricato, X. Li, H. P. Hratchian, A. F. Izmaylov, J. Bloino, G. Zheng, J. L. Sonnenberg, M. Hada, M. Ehara, K. Toyota, R. Fukuda, J. Hasegawa, M. Ishida, T. Nakajima, Y. Honda, O. Kitao, H. Nakai, T. Vreven, J. J. A. Montgomery, J. E. Peralta, F. Ogliaro, M. Bearpark, J. J. Heyd, E. Brothers, K. N. Kudin, V. N. Staroverov, R. Kobayashi, J. Normand, K. Raghavachari, A. Rendell, J. C. Burant, S. S. Iyengar, J. Tomasi, M. Cossi, N. Rega, J. M. Millam, M. Klene, J. E. Knox, J. B. Cross, V. Bakken, C. Adamo, J. Jaramillo, R. Gomperts, R. E. Stratmann, O. Yazyev, A. J. Austin, R. Cammi, C. Pomelli, J. W. Ochterski, R. L. Martin, K. Morokuma, V. G. Zakrzewski, G. A. Voth, P. Salvador, J. J. Dannenberg, S. Dapprich, A. D. Daniels, Ö. Farkas, J. B. Foresman, J. V. Ortiz, J. Cioslowski and D. J. Fox, *Gaussian 09, Revision D.01*, Gaussian, Inc., Wallingford, CT, 2013.
58 R. G. Gilbert and S. C. Smith, *Theory of Unimolecular and Recombination Reactions*, Blackwell Scientific, Carlton, Australia, 1990.
59 K. A. Holbrook, Michael J. Pilling and S. H. Robertson, *Unimolecular Reactions*, Wiley, New York, 1996.
60 S. J. Klippenstein and L. B. Harding, *J. Phys. Chem. A*, 2000, **104**, 2351–2354.
61 L. K. Huynh, H. R. Zhang, S. Zhang, E. Eddings, A. Sarofim, M. E. Law, P. R. Westmoreland and T. N. Truong, *J. Phys. Chem. A*, 2009, **113**, 3177–3185.
62 D. R. Glowacki and M. J. Pilling, *Chem. Phys. Chem.*, 2010, **11**, 3836–3843.
63 G. da Silva, *J. Phys. Chem. A*, 2012, **116**, 5317–5324.
64 D. W. Chandler and J. A. Miller, *J. Chem. Phys.*, 1984, **81**, 455–464.
65 J. A. Miller and D. W. Chandler, *J. Chem. Phys.*, 1986, **85**, 4502–4508.
66 J. A. Miller and S. J. Klippenstein, *J. Phys. Chem. A*, 2006, **110**, 10528–10544.
67 J. A. Miller, S. J. Klippenstein and S. H. Robertson, *J. Phys. Chem. A*, 2000, **104**, 7525–7536.
68 L. K. Huynh, H. R. Zhang, S. Zhang, E. Eddings, A. Sarofim, M. E. Law, P. R. Westmoreland and T. N. Truong, *J. Phys. Chem. A*, 2009, **113**, 3177–3185.
69 W. T. Duncan, R. L. Bell and T. N. Truong, *J. Comput. Chem.*, 1998, **19**, 1039–1052.
70 G. J. R. Aroeira, A. S. Abbott, S. N. Elliott, J. M. Turney and H. F. Schaefer, *Phys. Chem. Chem. Phys.*, 2019, **21**, 17760–17771.
71 L. Chen, Y. Huang, Y. Xue, Z. Shen, J. Cao and W. Wang, *Atmos. Chem. Phys.*, 2019, **19**, 4075–4091.
72 N. A. I. Watson, J. A. Black, T. M. Stonelake, P. J. Knowles and J. M. Beames, *J. Phys. Chem. A*, 2019, **123**, 218–229.
73 W.-m Wei, S. Hong, W.-j Fang, R.-h Zheng and Y.-d Qin, *Theor. Chem. Acc.*, 2019, **138**, 13.
74 R. S. Zhu and M. C. Lin, *J. Phys. Chem. A*, 2000, **104**, 10807–10811.
75 C. Sun, Y. Liu, B. Xu, Y. Zeng, L. Meng and S. Zhang, *J. Chem. Phys.*, 2013, **139**, 154307.